

Elsevier Editorial System(tm) for Measurement  
Manuscript Draft

Manuscript Number:

Title: Conversion of a digital camera into a non-contact colorimeter for use in the field of granite conservation

Article Type: Research Paper

Keywords: CIELAB system; CMOS camera; color calibration; cultural heritage; granite; ornamental stone; RGB values.

Corresponding Author: Dr. Patricia Sanmartín,

Corresponding Author's Institution: University of Santiago de Compostela

First Author: Patricia Sanmartín

Order of Authors: Patricia Sanmartín; Elisabet Chorro; Daniel Vázquez-Nion; Francisco M Martinez-Verdu; Beatriz Prieto

Abstract: In this study, a digital CMOS camera was calibrated for use as a non-contact colorimeter for measuring the color of granite artworks. The low chroma values of the granite, which yield similar stimulation of the three color channels of the camera, proved to be the most challenging aspect of the task. The appropriate parameters for converting the device-dependent RGB color space into a device-independent color space were established. For this purpose, the color of a large number of Munsell samples (corresponding to the previously defined color gamut of granite) was measured with a digital camera and with a spectrophotometer (reference instrument). The color data were then compared using the CIELAB color formulae. The best correlations between measurements were obtained when the camera works to 10-bits and the spectrophotometric measures in SCI mode. Finally, the calibrated instrument was used successfully to measure the color of six commercial varieties of granite.

Suggested Reviewers: Federica Villa

Dipartimento di Scienze per gli Alimenti, la Nutrizione e l'Ambiente, Università degli Studi di Milano  
federica.villa@unimi.it

Ana Zelia Miller

Centre for Petrology and Geochemistry (CEPGIST), Technical University of Lisbon  
anamiller@gmail.com

Remigio Paradelo

Centre AgroParisTech : Paris-Grignon, Centre AgroParisTech : Paris-Grignon  
remigio.paradelo@agroparistech.fr

Nicolas Concha-Lozano

Scientifique de laboratoire, Institut universitaire romand de Santé au Travail (IST)  
nicolas.concha-lozano@chuv.ch

Marcos Paradelo

Department of Agroecology , Aarhus University

[mparadelo@uvigo.es](mailto:mparadelo@uvigo.es)

Harvard University, Cambridge (Massachusetts). March 26, 2014

Dear Dr. K.T.V. Grattan  
Editor-in-Chief of *Measurement*  
Journal of the International Measurement Confederation (IMEKO),

We send you a copy of our original manuscript entitled “**Conversion of a digital camera into a non-contact colorimeter for use in the field of granite conservation**”, written by Patricia Sanmartín, Elisabet Chorro, Daniel Vázquez-Nion, Francisco Miguel Martínez-Verdú and Beatriz Prieto which has not been submitted for publication elsewhere. We would be very pleased to be considered for its publication in **Measurement**, since it contributes to development and the specific application of remote color measurement on granite rocks, and in this sense is concerned with the scope of this journal.

Awaiting news, we hope that the manuscript will be judged suitable for publication. We look forward to hearing from you at your earliest convenience.

Sincerely,

Patricia Sanmartín  
BSc, PhD  
Postdoctoral Researcher from I2C Plan (Mode A)  
Departamento de Edafología e Química Agrícola  
Facultade de Farmacia. Universidade de Santiago de Compostela  
15782. Santiago de Compostela (A Coruña, Spain)

Current address:  
Laboratory of Applied Microbiology  
Harvard School of Engineering and Applied Sciences (SEAS)  
HARVARD  
29 Oxford Street. Cambridge, MA 02138. USA

**Highlights:**

- We develop the fine-tuning of a method for the remote color measurement of granite.
- It is reported the description of a affordable methodology with digital camera.
- We estimate the effect of uncertainty on the measurement result.
- Choice combination of camera and spectrophotomer minimizes uncertainty of measurement.
- The calibrated camera was successfully used on granite stones.

Potential Reviewers:

- Federica Villa. Università degli Studi di Milano (federica.villa@unimi.it).
- Ana Zelia Miller. Technical University of Lisbon (anamiller@gmail.com).
- Remigio Paradelo. Centre AgroParisTech : Paris-Grignon (remigio.paradelo@agroparistech.fr).
- Nicolas Concha-Lozano. Institut universitaire romand de Santé au Travail (IST) (nicolas.concha-lozano@chuv.ch).
- Marcos Paradelo. Aarhus University (mparadelo@uvigo.es).

## **Conversion of a digital camera into a non-contact colorimeter for use in the field of granite conservation**

Patricia Sanmartín<sup>1\*</sup>, Elisabet Chorro<sup>2</sup>, Daniel Vázquez-Nion<sup>1</sup>, Francisco Miguel Martínez-Verdú<sup>2</sup>, Beatriz Prieto<sup>1</sup>

1. Departamento de Edafología y Química Agrícola. Facultad Farmacia. Universidad de Santiago de Compostela, 15782 - Santiago de Compostela, Spain.

2. Color & Vision Group, University Institute of Physics Applied to Sciences and Technologies. University of Alicante, San Vicente del Raspeig, 03690-Alicante, Spain.

\*Corresponding author: Patricia Sanmartín

Departamento de Edafología y Química Agrícola

Facultad de Farmacia. Campus Vida

Universidad de Santiago de Compostela

15782 Santiago de Compostela. SPAIN

Telephone: +34 881 814920 Fax: +34 881 815106

E-mail address: [patricia.sanmartin@usc.es](mailto:patricia.sanmartin@usc.es)

<http://www.usc.es>

Current address:

Prof. Ralph Mitchell's Laboratory of Applied Microbiology

Engineering Science Building, 58 Oxford St. Cambridge, MA 02138. USA

Harvard School of Engineering and Applied Sciences (SEAS)

HARVARD

1 **Abstract**

2 In this study, a digital CMOS camera was calibrated for use as a non-contact  
3 colorimeter for measuring the color of granite artworks. The low chroma values of the  
4 granite, which yield similar stimulation of the three color channels of the camera,  
5 proved to be the most challenging aspect of the task. The appropriate parameters for  
6 converting the device-dependent RGB color space into a device-independent color  
7 space were established. For this purpose, the color of a large number of Munsell  
8 samples (corresponding to the previously defined color gamut of granite) was measured  
9 with a digital camera and with a spectrophotometer (reference instrument). The color data  
10 were then compared using the CIELAB color formulae. The best correlations between  
11 measurements were obtained when the camera works to 10-bits and the  
12 spectrophotometric measures in SCI mode. Finally, the calibrated instrument was used  
13 successfully to measure the color of six commercial varieties of granite.

14

15 **Keywords:** CIELAB system; CMOS camera; color calibration; cultural heritage;  
16 granite; ornamental stone; RGB values.

17

18

19

20

21

22

23

24

25  
26  
27  
28  
29  
30  
31  
32  
33  
34  
35  
36  
37  
38  
39  
40  
41  
42  
43  
44  
45  
46  
47  
48  
49  
50  
51  
52  
53  
54  
55  
56  
57  
58  
59  
60  
61  
62  
63  
64  
65  
66  
67

## 1. Introduction

Color is one of the most important visual properties of ornamental and monumental stone. Color changes caused by weathering and decay greatly influence the aesthetic value of stone. In some cases, the extent of such change can be detected by the naked eye. However, this type of assessment can be very subjective, and color quantification with colorimeters and spectrophotometers is more accurate (e.g. [1-6]). These devices are capable of highly reproducible color measurements in a device-independent color space, such as CIE-XYZ or CIE-L\*a\*b\*, in which the coordinates are specific to a particular color. However, there are some limitations to the use of contact color measuring devices for buildings and monuments, the main one of which is being able to reach the target object with the instrument. These devices are also more expensive and complex than other non-dedicated color measuring devices (digital cameras and scanners and even mobile-phone cameras). Finally, as the field of view of contact color devices is limited, measurement of the color of heterogeneous surfaces produces unrealistic values. Digital cameras can be used to overcome these limitations because (i) the field of view is only limited by the size of the appropriately illuminated area, (ii) contact with the target object is not required, and (iii) they encode each point of the entire surface simultaneously, thus quantifying surface characteristics and defects.

Scanners and digital cameras essentially operate via a matrix of optoelectronic sensors that transform variations in light intensity into digital signals. Therefore, they only detect changes in light intensity, not color. To encode color, image-capturing devices require three different filters in addition to the sensors. These filters usually have spectral bands in the red (R), green (G) and blue (B) regions, and therefore the encoded values are RGB digital values. RGB is a device-dependent color space as the filters and other parameters are specific to individual cameras and can be changed with camera settings such as the spectral exposure level, white balance and the dynamic range. As RGB values cannot be transformed to XYZ or L\*a\*b\* values directly by using a standard formula, a transformation that defines the mapping between RGB digital values and a device independent color space is essential to enable the relation between camera sensor responses and visual perception to be established. This process is known as camera characterization [7-9]. Camera characterization is used to predict color acquisition and recording of the color content of an image according to luminance, hue and chroma scales [10]. Several camera characterization techniques have been used with the aim of developing a model (and estimating its parameters) for obtaining L\*a\*b\* color measurements from RGB digital values (e.g. [7, 8, 11-15]). In general, the techniques can be divided into two categories: (1) *spectral characterization*, which measures the three spectral-sensitivity functions for the red-green-blue (RGB) channels and requires a monochromator and a radiance meter [16]; and (2) *colorimetric characterization*, which involves mathematical transformations that yield the tristimulus values from the digital values and which require use of a reference target that contains a certain number of color samples. In the present study, we used the latter color target-

68 based approach, which only requires a certain number of color samples and is, therefore,  
69 a more practical method [7]. We chose target-based characterization procedure  
70 described by Hong et al. [7], which is based on polynomial modeling. This calibration  
71 model has been used successfully in nearly two hundred scientific papers with different  
72 objectives, e.g., to determine how facial skin coloration affects perceived health of  
73 human faces [17, 18] and for use in dental color matching [19].  
74

75 In the field of lithology and textured building materials, the image captured by the  
76 camera is usually processed by different segmentation strategies. For example, one  
77 innovative application focuses on the segmentation of decay zones from images of stone  
78 materials [20, 21]. Another strategy enables improvement and semi-automatization of  
79 the study of chemical decay causing visible changes in color of some regions [22]. A  
80 portable stereo active vision system (AVS) has also been specifically designed to  
81 perform on-site processing of the data acquired in the field of cultural heritage  
82 conservation [23]. Moreover, the digital decorrelation of RGB images by Principal  
83 Components Analysis (PCA) enables contrast enhancement of minority elements  
84 apparently absent from the initial RGB digital image [24-27]. Camera characterization  
85 has been used in very few studies, including that of Chorro et al. [28], who used the  
86 sRGB model to predict the CIE-XYZ tristimulus values depending on the RGB digital  
87 data, with the final aim of quantifying color changes in the appearance of a paving stone  
88 (marble) in relation to the viewing distance. More recently, Concha-Lozano et al. [29]  
89 used spectroradiometric measurements to calibrate a camera in order to establish the  
90 color ranges within which replacement of biotrititic limestone in medieval walls will  
91 be imperceptible. Nevertheless, to our knowledge, camera characterization has not  
92 previously been reported for granite. Measurement of the color of granite is complicated  
93 by the low chroma and spatially heterogeneous color, which is formed by the different  
94 colors of the constituent minerals. There is great interest in measuring the color of  
95 granite because, amongst other reasons, granite is one of the most commonly used types  
96 of igneous rock owing to its abundance and great variety of color and textures, and  
97 because it is a major construction material in European historical buildings and  
98 monuments [30].  
99

100 The present study focused on developing a method of RGB digital camera colorimetric  
101 characterization for studying stone, specifically granite, with low chroma color. The  
102 nearly neutral colors of granite yield similar stimulation of the three color channels of  
103 the camera (red, green and blue), which makes the task in hand particularly challenging.  
104 For the first time, the settings of a digital camera have been adjusted to obtain the  
105 camera response closest to that of the reference instrument (spectrophotometer) for  
106 granite color measurement using the CIELAB system. The developed method was  
107 successfully used to measure the color of granite samples. The process involves  
108 conversion of the digital camera into a non-contact colorimeter. This is of particular  
109 interest in the field of stone conservation and manufacturing of artificial stones and  
110 ceramics with different colors and textures, in which innovative non-invasive tools for  
111 monitoring the aesthetic changes in stone surfaces are required.

## 2. Experimental

### 2.1. Fine-tuning of the camera calibration method

The methodology developed for estimating the RGB→L\*a\*b\* transformation consisted of two parts. In the first part, we determined the appropriate settings and working conditions of the acquisition system (camera) and reference instrument (spectrophotometer). In the second part, we selected a large set of Munsell matte and glossy samples corresponding to the previously defined color gamut of granite [31]. The colors of these samples were measured using both devices under the conditions indicated in the first part. The digital images were obtained with the following image acquisition system (*Figure 1*):

- PixeLINK PL-A782 color digital camera, 2008 (suitable for industrial use), with CMOS sensor architecture, 6.6 Mega Pixels of resolution and a user-selectable 8 or 10-bit output. The camera was placed vertically at a distance of 112 cm from the sample. The angle between the axis of the camera and the source of illumination was approximately 45°. Thus, following the CIE nomenclature [32], the measurement geometry was 45°x90° or 45/0, which is very common in industrial applications when diffuse illumination is not available.
- Camera lens: Fujinon CF50HA-1, 50 mm focal length, 1", 1.5 Megapixel, with manual iris and focus.
- Lighting was achieved with Kaiser RB-5004-HF high frequency daylight copy light set with four Oxram Dulux L 36W/954 fluorescent light tubes (41.5 cm in length), with a correlated color temperature of 5400 K (natural daylight) and a color rendering index ( $R_a$ ) close to 90%.
- The room where images were taken was totally dark and a black cloth was placed on the floor under the table used as the sample stand, to minimize background light.
- The size of the captured images was 240 pixels (width) by 192 pixels (height). The pixel size was 347 x 375  $\mu\text{m}^2$ . The images were captured and imported by connecting the camera to the USB port of an Acer Aspire 1350 computer.
- The camera settings used in the present study are summarized in *Figure 2*. The main purpose of this step was to maintain constant any software camera control (white balance, exposure time, gain, etc) to obtain a stable, reliable and reproducible RGB color space, although this would presumably limit the dynamic range of luminance of the camera [33].

The lighting level, and its uniformity, is critical for image acquisition, so that the camera can deliver meaningful, repeatable data [34]. Therefore, the lighting map for the reference target needs to be as spatially and temporally uniform as possible. The uniformity of light intensity was tested using a radiometer (DHD 2302.0, HERTER) (*Figure 3*).

155 However, the combination of lens aperture size and exposure time determines the  
156 amount of light reaching the CMOS sensor of the camera. Obviously, the signals  
157 generated by the CMOS sensor vary with the amount of light reaching CMOS sensor.  
158 Therefore, both aperture size ( $f/4$ ) and exposure time (99.537) were fixed during the  
159 period of image acquisition. We also totally occluded the camera-lens aperture for the  
160 black reference, and we captured a standard white reference plate for the white  
161 reference.

162

163 The camera is capable of both 8-bit depth and 10-bit depth linear data acquisition; both  
164 were used in the present study. 8-bit data can hold  $2^8 = 256$  possible values ranging  
165 from 0 to 255. For an RGB image in which the values are 8-bit unsigned integers, 0 0 0  
166 represents black, 255 255 255 represents white, 255 0 0 represent red, 0 255 0  
167 represents green, and 0 0 255 represents blue. 10-bit data yields  $2^{10} = 1024$  possible  
168 values, ranging from 0 to 1023. For an RGB image in which the values are 10-bit  
169 unsigned integers, 0 0 0 represents black, 1023 1023 1023 represents white, 1023 0 0  
170 represents red, 0 1023 0 represents green, and 0 0 1023 represents blue. Special  
171 attention was paid to setting the exposure to avoid any “color clipping” for the white  
172 reference, i.e., saturation of one or more of the three RGB channels, obtaining R, G or B  
173 values above 255 with 8-bit data and 1023 with 10-bit data [7, 13].

174

175 The spectrophotometer used was a portable spectrophotometer (Konica Minolta CM-  
176 700d) equipped with CM-S100w (SpectraMagic™ NX) software. The measuring  
177 conditions were illuminant D65, observer  $2^\circ$  and a 3-mm diameter viewing area.  
178 Measurements were made in both specular component included (SCI) and specular  
179 component excluded (SCE) modes to determine which mode approximates better to the  
180 camera vision. The SCI mode, in which the gloss trap of the spectrophotometer is  
181 closed, includes the total reflectance (considering both specular and diffuse reflections);  
182 the SCE mode, in which the gloss trap is open, includes the diffuse reflectance and  
183 excludes most of the specular component and is therefore more sensitive to color  
184 differences due to differences in surface roughness [31, 35]. It is generally accepted in  
185 the field of color science that the SCE mode approximates the view with the naked eye  
186 and the SCI mode is adequate for analyzing the intrinsic color of objects [31, 36].

187

188 In attempting to adjust the camera settings to make the camera response more similar to  
189 the reference-instrument response in the CIELAB system, standard color targets  
190 consisting of an assortment of color patches are commonly applied. The Gretag  
191 Macbeth color-checker color rendition chart [37] is one of the most commonly used,  
192 although it consists of only 24 patches. In some cases, as in the second part of our  
193 camera characterization method, a customized characterization target, consisting of a  
194 large number of patches, was designed and applied. Thus, a set of samples (212 Munsell  
195 color charts, 125 from the glossy and 87 from the matte collection), corresponding to  
196 the three-dimensional color area of the CIELAB space, in which the color of the  
197 ornamental granites is defined [31] was selected. In each of the 212 color samples, the  
198  $L^*a^*b^*$  color values were measured using the portable spectrophotometer under the

199 measuring conditions described above. One reading was taken per sample. An RGB  
200 digital image was also taken of each Munsell sample/chip. The digital camera was  
201 placed orthogonally to the Munsell sample. The field of view of the camera was fully  
202 occupied by a single Munsell chip. Thus, 212 RGB measurements, i.e., R, G and B  
203 color values, were obtained. Note that the granite color is located in the nearly neutral  
204 region of CIELAB color space, far from the highly saturated colors like intense or pure  
205 yellows, reds and greens. This makes it difficult for the instrument to measure the color,  
206 as the nearly neutral colors yield similar stimulation of the three color channels (red,  
207 green, and blue) of the camera, and the differences between these colors constitute small  
208 variations in a high nearly constant background signal [10].

## 210 2.2. Performance testing and verification of the resulting calibration

211  
212 To confirm selection of the camera working conditions, the method described in Section  
213 2.1 was applied to the color characterization of granite samples. Six commercial  
214 varieties of granite (*Aldán, Blanco Cristal, Grissal, Monte Enxa, Rosa Porriño* and  
215 *Silvestre*) were considered. Data on the origin, geochemistry and textural and mineral  
216 characteristics of each type of granite are shown in **Table 1**. Five square specimens (25  
217 or 36cm<sup>2</sup>) of each type of granite were prepared with a honed surface finish. An image  
218 of each specimen was taken using the image acquisition system described in Section  
219 2.1. During the process, each of the samples was placed on the marked area of a light  
220 table. The measurement area in the specimens was approximately 6.25 cm<sup>2</sup> (width, 25  
221 mm and length, 25 mm). The color of granite samples was then measured with a  
222 portable spectrophotometer (Konica Minolta CM-700d) equipped with CM-S100w  
223 (SpectraMagic<sup>TM</sup> NX) software, following the working methodology designed by  
224 Prieto et al. [38]. The measuring conditions and specular component modes were the  
225 same as those used to measure the Munsell samples (see Section 2.1).

## 226 3. Results and discussion

227 The stability of the light source was evaluated prior to establishing the color  
228 measurement protocol for the study. Figure 3 shows the light levels across the table top.  
229 The light was not completely homogeneous and varied from 1560 ± 20 lx at the upper  
230 center to 2400 ± 20 lx to the right and left of the middle-center. An area of the table  
231 where the percentage of light level (in lx) did not vary by more than 3% was marked.  
232 The average level of lighting was 1780 ± 20 lx within this area, which is where the  
233 images were captured.

234  
235 The color of the 212 test samples (Section 2.1) was measured using both devices. Hong  
236 et al. [7] noted that better results can be achieved if more terms (e.g. R<sup>2</sup>, G<sup>2</sup>, B<sup>2</sup>, etc) are  
237 included to the matrix derived by the characterization process of the digital camera. In  
238 the present study, a third order polynomial (matrix with 20 terms) was used. This can be  
239 expressed as follows [9]:

240

$$\mathbf{D} = \begin{bmatrix} L_1^* & a_1^* & b_1^* \\ \vdots & \vdots & \vdots \\ L_n^* & a_n^* & b_n^* \end{bmatrix} \quad (1)$$

$$\mathbf{V} = \begin{bmatrix} 1 & R_1 & G_1 & B_1 & R_1 G_1 & R_1 B_1 & \dots & R_1^3 & G_1^3 & B_1^3 \\ \vdots & \vdots & \vdots & \vdots & \vdots & \vdots & \dots & \vdots & \vdots & \vdots \\ 1 & R_n & G_n & B_n & R_n G_n & R_n B_n & \dots & R_n^3 & G_n^3 & B_n^3 \end{bmatrix} \quad (2)$$

$$\mathbf{D} = \mathbf{M} \cdot \mathbf{V} \quad (3)$$

$$\mathbf{M} = [m_{ij}]_{3 \times 20} = \left[ (\mathbf{V}^t \cdot \mathbf{V})^{-1} \mathbf{V}^t \cdot \mathbf{D} \right]^t \quad (4)$$

where  $M$  is the matrix with the transformation polynomial coefficients characterizing the camera,  $\{R_n, G_n, B_n\}$  are the digital levels of the training color patches (i.e. 212 color charts-Section 2.1) measured by the camera and  $\{L_n^*, a_n^*, b_n^*\}$  are the CIE- $L^*a^*b^*$  values of the training set (i.e. 212 color charts-Section 2.1) measured by the spectrophotometer. Finally, transformation of the RGB values was achieved by using the following equation:

$$\begin{bmatrix} L^* \\ a^* \\ b^* \end{bmatrix} = [m_{ij}]_{3 \times 20} \cdot \begin{bmatrix} 1 \\ R \\ G \\ B \\ RG \\ \dots \\ B^3 \end{bmatrix}_{20 \times 1} \quad (5)$$

The absolute color measurement by the camera, calculated using Eq. (5), in both 8 and 10-bits of color depth, was compared with the external reference provided by the spectrophotometer, in both specular component included (SCI) and excluded (SCE) modes. The CIELAB coordinates of each measured chip, obtained separately by the camera and the reference instrument were compared, taking into account the classical CIELAB formula ( $\Delta E_{ab}^*$ ) and the other color difference formulae based on CIELAB space ( $\Delta E_{94}$ ,  $\Delta E_{00}$  and CMC). The results obtained are shown in **Table 2**, which includes the average, maximal and minimal values of the computed total color differences, *viz.*  $\Delta E_{ab}^*$ ,  $\Delta E_{94}$  (2:1:1),  $\Delta E_{94}$  (1:1:1),  $\Delta E_{00}$  (2:1:1),  $\Delta E_{00}$  (1:1:1), CMC (2:1) and CMC (1:1). No equivalence of scale factor was found in the values calculated using the different formulae considered, as reported by Prieto et al. [38] on comparing the results obtained by measuring granite samples with the different reading areas (or measuring head sizes) of a spectrophotometer and a colorimeter. It is difficult to specify

271 admissible color differences between devices, because most recommendations on color  
272 differences refer to situations in which the colors of different objects are measured  
273 under the same illuminant, unlike in the present study (Section 2.1). The color-tolerance  
274 concept is based on color discrimination, which largely depends on observational  
275 conditions. In this case, we should take into account that the color of the sample was  
276 viewed with different illumination, leading to greater color tolerance. For instance,  
277 analysis of the color differences in both natural and artificial objects over one day  
278 revealed values exceeding 3 CIELAB units when the color of the objects under the  
279 maximum solar elevation was compared with that at twilight [39]. Based on these  
280 findings, consideration of 1 CIELAB unit as the visual color difference threshold or just  
281 noticeable difference (jnd), which constitutes the lower limit of perception in an  
282 individual with normal color vision [35, 40] appears too strict in this case. Likewise  
283 1.75 CIELAB units, considered as the suprathreshold color-difference [41]. Thus, we  
284 decided to consider for evaluation of the results perceptual limits starting from 3  
285 CIELAB units and taking into account the following established thresholds: (1) the  
286 normal color tolerance, specified by Lozano [42] as being between 2.8 and 5.6 CIELAB  
287 units (according to the usual conversion factors between color-difference units [40]); (2)  
288 the acceptable color tolerance of 3 CIELAB units [43, 44]; (3) the normal limit of  
289 perception in industrial or technical applications of 5 CIELAB units [45-47], and (4) the  
290 perceptible but acceptable difference in color of 6 CIELAB units considered by  
291 Hardeberg [48]. We found that the average total color differences obtained, ranging  
292 from 1.9 to 1.1 CIELAB units (**Table 2**), are nearly undetectable to the untrained eye.  
293 The maximal total color differences, with values ranging from 3.7 to 6.9 CIELAB units,  
294 must be considered virtually acceptable for most industrial applications. Furthermore,  
295 the color difference formulae based on CIELAB space include three parametric factors,  
296  $k_L$ ,  $k_C$  and  $k_H$ , which are correction terms for the variation in experimental conditions.  
297 Under reference conditions, these are all set at 1 [32]. However, in the present study, the  
298 illumination conditions were not reference conditions and the samples were not  
299 homogeneously colored. For textured samples, it is not clear which values should be  
300 used for the parametric factors [49-51]. Considering an increase in the relative  
301 contribution of the lightness term ( $k_L$  parametric factor 2, instead of 1) in the color  
302 difference formulae, the maximum value decreased greatly by between 2 and 3  
303 CIELAB units, and only reached values of between 3.7 and 3.9 CIELAB units (**Table**  
304 **2**).

305

306 In order to select the optimal camera conditions, the lowest maximal value of the total  
307 color differences was used as a selection criterion. The optimal camera conditions,  
308 according to this criterion, for 8- and 10-bit data, are highlighted in **Table 2** for each  
309 color difference formulae calculated using SCI or SCE data. Taking into account all of  
310 the data, the smallest differences between the camera and spectrophotometer were  
311 obtained on comparing SCI spectrophotometric data with 10-bit camera data.  
312 Consequently, the digital camera 10-bit depth linear data acquisition is the best for our  
313 purpose and should be compared with SCI spectrophotometric data.

314

315 In the cultural heritage field, most colorimetric measurements are used to estimate color  
316 differences (e.g. [6, 52]). Therefore, to calibrate a digital camera as a colorimeter for use  
317 in this field, it is advisable to explore the discriminatory capacity of the camera and its  
318 reliability for measuring small differences between very similar colors. A certain  
319 number of color differences between pairs of nearest-neighbor chips were calculated  
320 separately by both the camera and the reference instrument, according to the classical  
321 CIELAB formula ( $\Delta E^*_{ab}$ ) and other color difference formulae based on the CIELAB  
322 space ( $\Delta E_{94}$ ,  $\Delta E_{00}$  and CMC). Comparison of the results obtained with the camera and  
323 the reference instrument indicated the discrepancy between the two devices. This  
324 discrepancy was used to test the reliability of the camera performance and was  
325 compared with the precision and tolerance of the devices (**Tables 3 and 4**). More than  
326 half of the absolute discrepancies exceed the suprathreshold value for visual  
327 discrimination of 0.887 CIELAB units [41]. Nonetheless, the values of the relative  
328 discrepancy were very low and although the absolute discrepancy exceeded the  
329 uncertainty or precision of both devices, it remained within the camera tolerance ( $1.32 \pm$   
330  $1.06$  vs.  $2.4$  CIELAB units). Thus, the camera and reference instrument showed a high  
331 degree of consistency in the estimation of small color differences, and therefore the  
332 camera performed well [53].

333

334 The selected camera working conditions were then used to characterize the color of six  
335 commercial varieties of granite (*Aldán*, *Blanco Cristal*, *Grissal*, *Monte Enxa*, *Rosa*  
336 *Porriño* and *Silvestre*). The results obtained (*Figure 4*) appeared sufficiently accurate  
337 and reliable: considering the set of samples, regardless of type of granite and granite  
338 sample, the total color difference ( $\Delta E^*_{ab}$ ) between the measured granite color (using the  
339 spectrophotometer in specular component included (SCI) mode) and the estimated  
340 granite color (using the digital camera with 10-bits data acquisition) was generally  
341 below 6 CIELAB units. Specifically, the  $\Delta E^*_{ab}$  values ranged between 2.7 and 5.5  
342 CIELAB units for *Grissal* and 3.4 and 5.1 CIELAB units for *Blanco Cristal*, indicating  
343 that, with the measurement method used, the best results were obtained with achromatic  
344 rocks. The values of  $\Delta E^*_{ab}$  for *Monte Enxa* and *Rosa Porriño* ranged from 4.4 to 6.6  
345 and from 4.3 to 7.0, respectively. These were the largest color differences reached in the  
346 study and corresponded to those types of granite in which the color is farthest from the  
347 achromatic area. Intermediate values of  $\Delta E^*_{ab}$  were obtained for *Aldán*, with values  
348 within the range of 3.0 - 6.5 CIELAB units, and for *Silvestre*, with values within the  
349 range 3.3 - 5.5 CIELAB units. In this case, differences of 6 CIELAB units cannot be  
350 considered high as two different devices with different lighting conditions were used.  
351 For granite color measurements, differences of nearly 3 CIELAB units are obtained,  
352 even when using the same device with different measuring heads [38]. Moreover, the  
353 limits of perception are usually calculated for homogeneous samples (in terms of color  
354 and texture) (for further details, see, e.g. [54]), unlike the granite samples that were the  
355 target of the present study.

356 **4. Conclusions**

357 A calibration procedure was developed for granite color measurement using a non-  
358 contact device (a CMOS digital camera). Working conditions for the reference  
359 instrument (spectrophotometer) and the digital camera were examined to ensure the best  
360 possible correlation between both devices. An improvement was obtained by quantizing  
361 the camera RGB values to 10-bits relative to those recorded in 8-bits. Likewise, better  
362 results were achieved with the specular component included (SCI) mode than with the  
363 specular component excluded (SCE) mode in the reference instrument  
364 (spectrophotometer).

365

366 The resulting calibration was successfully applied to six commercial varieties of granite,  
367 and the differences between data obtained with the reference instrument and with the  
368 camera calibrated as colorimeter were no higher than 6 CIELAB units.

369

370 This method, which enables RGB data to be expressed as device independent L\*a\*b\*  
371 data, without introducing a noticeable amount of error, is sufficiently adaptable to be  
372 transposed to any computer vision system that can produce consistent RGB source data.  
373 The method can be used in many industrial applications using textured colored  
374 materials and products. Apart from the fact that contact is not required for the color  
375 measurement, the other main advantage is the flexibility afforded by the choice of the  
376 size of the area to be characterized, which can range from small areas (347 x 375 pixel  
377 size  $\mu\text{m}^2$ ) to areas as large as allowed by the lens size.

378 **Acknowledgements**

379 The present study was financially supported by the Xunta de Galicia  
380 (09TMT014203PR) and the European Union and Spanish Ministry of Economy and  
381 Competitiveness under grants DPI2008-06455-C02-02 and DPI2011-30090-C02-02.  
382 Dr. Patricia Sanmartín acknowledges a scholarship for postgraduate studies abroad  
383 (2012 Call) from Barrié de la Maza Foundation. She is currently supported by a  
384 postdoctoral contract within the framework of the 2011-2015 Galician Plan for  
385 Research, Innovation and Growth (Plan I2C) for the year 2012.

386

387 **References**

388 [1] D.L. MacAdam, Colour Measurement –Theme and Variations, Second Revised  
389 Edition, Springer-Verlag, 1985.

390

391 [2] H.A.Viles, M.P. Taylor, T.J.S. Yates, S.W. Massey, Soiling and decay of NMEP  
392 limestone tablets, *Sci Total Environ* 292 (2002) 215–229.

393

394 [3] H.A. Viles, A.A. Gorbushina, Soiling and microbial colonization on urban roadside  
395 limestone: a three year study in Oxford, England, *Build Environ* 38 (2003) 1217–1224.

396

- 397 [4] M. Thornbush, H.A. Viles, Changing patterns of soiling and microbial growth on  
398 building stone in Oxford, England after implementation of a major traffic scheme, *Sci*  
399 *Total Environ* 367 (2006) 203–211.  
400
- 401 [5] C.M. Grossi, P. Brimblecombe, R.M. Esbert, F.J. Alonso, Color changes in  
402 architectural limestones from pollution and cleaning, *Color Res Appl* 32 (2007) 320–  
403 331.  
404
- 405 [6] P. Sanmartín, D. Vázquez-Nion, B. Silva, B. Prieto, Spectrophotometric color  
406 measurement for early detection and monitoring of greening on granite buildings,  
407 *Biofouling* 28(3) (2012) 329–338.  
408
- 409 [7] G. Hong, M.R. Luo, P.A. Rhodes, A study of digital camera colorimetric  
410 characterization based on polynomial modeling, *Color Res Appl* 26(1) (2001) 76–84.  
411
- 412 [8] R. Blasubramanian, Device characterization. In: Sharma, G. (ed.), *Digital Color*  
413 *Imaging Handbook*, Boca Raton: CRC Press, chap. 5, 2003.  
414
- 415 [9] F. Martínez-Verdú, E. Chorro, E. Perales, M. Vilaseca, J. Pujol, Camera based  
416 colour measurement. In: Gulrajani, M.J. (ed.), *Colour measurements: principles,*  
417 *advances and industrial applications*, New Delhi: Woodhead Publishing, chap. 6, 2010.  
418
- 419 [10] M.S. Millán, E. Valencia, M. Corbalán, 3CCD Camera's capability for measuring  
420 color differences: experiment in the nearly neutral region, *App Opt* 43(36) (2004) 6523–  
421 6535.  
422
- 423 [11] P.L. Vora, J.E. Farrell, J.D. Tietz, D.H. Brainard, Digital color cameras. 1.  
424 Response models. Tech Rep HPL-97-53. Hewlett-Packard Laboratory, Palo Alto,  
425 California, [http://www.hpl.hp.com\\_techreports\\_97\\_HPL-97-53.html](http://www.hpl.hp.com_techreports_97_HPL-97-53.html), 1997.  
426
- 427 [12] P. Laflaquiere, D. Lafon, O. Eterradosi, P. Slangen, Characterization of color  
428 texture: CIEL\*a\*b\* calibration of CCD device. *Proc SPIE* 3409, 118–128, 1998.  
429
- 430 [13] F. Martínez-Verdú, J. Pujol, P. Capilla, Characterization of a digital camera as an  
431 absolute tristimulus colorimeter, *J Imaging Sci Technol* 47 (2003) 279–295.  
432
- 433 [14] K. Leon, D. Mery, F. Pedreschi, J. Leon, Color measurement in L\*a\*b\* units from  
434 RGB digital images, *Food Res Int* 39 (2006) 1084–1091.  
435
- 436 [15] R.E. Larraín, D.M. Schaefer, J.D. Reed, Use of digital images to estimate CIE  
437 color coordinates of beef, *Food Res Int* 41(4) (2008) 380–385.  
438
- 439 [16] R.S. Berns, M.J. Shyu, Colorimetric characterization of a desktop drum scanner  
440 using a spectral model, *J Electron Imaging* 4 (1995) 360–372.

441  
442  
443  
444  
445  
446  
447  
448  
449  
450  
451  
452  
453  
454  
455  
456  
457  
458  
459  
460  
461  
462  
463  
464  
465  
466  
467  
468  
469  
470  
471  
472  
473  
474  
475  
476  
477  
478  
479  
480  
481  
482  
483  
484

[17] I.D. Stephen, M.J.L. Smith, M.R. Stirrat, D.I. Perrett, Facial Skin Coloration Affects Perceived Health of Human Faces, *Int J Primatol* 30(6) (2009) 845-857.

[18] I.D. Stephen, V. Coetzee, D.I. Perrett, Carotenoid and melanin pigment coloration affect perceived human health, *Evol Hum Behav* 32(3) (2011) 216-227.

[19] L. Gómez-Robledo, N. López-Ruiz, M. Melgosa, A.J. Palma, L.F. Capitán-Vallvey, M. Sánchez-Marañón, Using the mobile phone as Munsell soil-colour sensor: An experiment under controlled illumination conditions, *Comput Electron Agr* 99 (2013) 200–208.

[20] R. Cossu, L. Chiappini, A color image segmentation method as used in the study of ancient monument decay, *J Cult Heritage* 5 (2004) 385–391.

[21] M.M. Cerimele, R. Cossu, Decay regions segmentation from color images of ancient monuments using fast marching method, *J Cult Heritage* 8 (2007) 170–175.

[22] L. Appolonia, V. Bruni, R. Cossu, D. Vitulano, Computer-aided monitoring of buildings of historical importance based on color, *J Cult Heritage* 7 (2006) 85–91.

[23] A. Balsamo, A. Chimienti, P. Grattoni, R. Nerino, G. Pettiti, M.L. Rastello, M. Spertino, Active vision applications to cultural heritage acquisition and monitoring, *J Cult Heritage* 7 (2006) 98–109.

[24] A.Z. Miller, N. Leal, L. Laiz, M.A. Rogerio-Candelera, R.J.C. Silva, A. Dionisio, M.F. Macedo, C. Saiz-Jimenez, Primary bioreceptivity of limestones used in Southern Europe monuments. In: Smith, B.J., Gomez-Heras, M., Viles, H.A., Cassar, J. (eds.), *Limestone in the Built Environment: Present Day Challenges for the Preservation of the Past*. *J Geol Soc, Special Publications* 331 (2010) 79-92.

[25] A.Z. Miller, M.A. Rogerio-Candelera, L. Laiz, J. Wierzchos, C. Ascaso, M.A. Sequeira Braga, M. Hernández-Mariné, A. Maurício, A. Dionísio, M.F. Macedo, C. Saiz-Jimenez, Laboratory-induced endolithic growth in calcarenites: biodeteriorating potential assessment, *Microbial Ecol* 60 (2010) 55-68.

[26] A.Z. Miller, M.A. Rogerio-Candelera, A. Dionísio, M.F. Macedo, C. Saiz-Jimenez, Microalgae as biodeteriogens of stone cultural heritage: qualitative and quantitative research by non-contact techniques. In: Columbus, F. (ed.), *Microalgae: Biotechnology, Microbiology and Energy*. Nova Science Publishers, pp.345-358, 2011.

[27] M.A. Rogerio-Candelera, Una propuesta no invasiva para la documentacion integral del arte rupestre (In Spanish). PhD thesis, Universidad de Sevilla, Spain, 2008.

- 485 [28] E. Chorro, E. Perales, D. de Fez, M.J. Luque, F.M. Martinez-Verdu, Application of  
486 the S-CIELAB color model to processed and calibrated images with a colorimetric  
487 dithering method, *Opt Express* 15 (2007) 7810–7817.  
488
- 489 [29] N. Concha-Lozano, D. Lafon, N. Sabiri, P. Gaudon, Color Thresholds for  
490 Aesthetically Compatible Replacement of Stones on Monuments, *Color Res Appl* 38(5)  
491 (2013) 356-363.  
492
- 493 [30] M.A. Vicente, J. Delgado Rodrigues, J. Acevedo, Degradation and Conservation of  
494 Granitic Rocks in Monument. Protection and Conservation of the European Cultural  
495 Heritage Research Report No. 5, European Commission: Brussels, Belgium, 1996.  
496
- 497 [31] P. Sanmartín, B. Silva, B. Prieto, Effect of surface finish on roughness, color and  
498 gloss of ornamental granites, *J Mater Civil Eng* 23(8) (2011) 1239–1248.  
499
- 500 [32] CIE Publication 15:2004. Commission Internationale de l’Eclairage, Vienna, 2004.  
501
- 502 [33] M. de Lasarte, M. Arjona, M. Vilaseca, F.M. Martínez-Verdú, J. Pujol, Luminance  
503 adaptation model for increasing the dynamic range of an imaging system based on a  
504 CCD camera, *Optik* 122(15) (2011) 1367-1372.  
505
- 506 [34] R.W.G. Hunt, *Measuring colour*, second edition. (Ellis Horwood series in applied  
507 science and industrial technology). Ellis Horwood Limited, 1995.  
508
- 509 [35] G. Wyszecki, W.S. Stiles, *Color Science. Concepts and Methods, Quantitative  
510 Data and Formulae*. John Wiley and Sons: New York, 1982.  
511
- 512 [36] Y. Hosoya, T. Shiraishi, T. Odatsu, T. Ogata, M. Miyazaki, J.M. Powers, Effects of  
513 specular component and polishing on color of resin composites, *J Oral Sci* 52(4) (2010)  
514 599-607.  
515
- 516 [37] C.S. McCamy, H. Marcus, J.G. Davidson, A Color-Rendition Chart, *J Appl  
517 Photogr Eng* 2(3) (1976) 95–99.  
518
- 519 [38] B. Prieto, P. Sanmartín, B. Silva, F. Martinez-Verdú, Measuring the color of  
520 granite rocks: A proposed procedure, *Color Res Appl* 35(5) (2010) 368-375.  
521
- 522 [39] J. Romero, J. Hernández-Andrés, J.L. Nieves, J.A. García, Color coordinates of  
523 objects with daylight changes, *Color Res Appl* 28 (2003) 25–35.  
524
- 525 [40] M. Melgosa, J.J. Quesada, E. Hita, Uniformity of some recent color metrics tested  
526 with an accurate color-difference tolerance dataset, *Appl Optics* 33(34) (1994) 8069-  
527 8077.  
528

- 529 [41] M. Melgosa, E. Hita, A.J. Poza, D.H. Alman, R.S. Berns, Suprathreshold color-  
530 difference ellipsoids for surface colors, *Color Res Appl* 22 (1997) 148–155.  
531
- 532 [42] R.D. Lozano, *El color y su medición*. AmericaLee: Buenos Aires, 1978.  
533
- 534 [43] R.S. Berns, Billmeyer and Saltzman's Principles of Color Technology, 3rd Ed.  
535 John Wiley and Sons: New York, 2000.  
536
- 537 [44] H.G. Völz, *Industrial color testing*. Wiley –VCH: Weinheim, 2001.  
538
- 539 [45] S. Palazzi, *Colorimetria, La scienza del colore nell'arte e nella tecnica*. Nardini  
540 Editore: Florence, Italy, 1995.  
541
- 542 [46] J.L. Nieves, F. Pérez-Ocón, J. Hernández-Andrés, J. Romero, Spectral-reflectance  
543 function recovery for improved colour-constancy experiments, *Displays* 23(5) (2002)  
544 213–222.  
545
- 546 [47] F. Cappitelli, E. Zanardini, G. Ranalli, E. Mello, D. Daffonchio, C. Sorlini,  
547 Improved methodology for bioremoval of black crusts on historical stone artworks by  
548 use of sulfate-reducing bacteria, *Appl Environ Microb* 72 (2006) 3733-3737.  
549
- 550 [48] J.Y. Hardeberg, *Acquisition and reproduction of color images: colorimetric and*  
551 *multispectral approaches*. PhD Thesis, Ecole Nationale Supérieure des  
552 *Telecommunications*, Paris, 1999.  
553
- 554 [49] CIE Publication 101:1993. *Parametric effects in colour-difference evaluation*.  
555 *Central Bureau of CIE*, Vienna, 1993.  
556
- 557 [50] M. Lucassen, P. Bijl, The CIE94 colour difference formula for describing visual  
558 detection thresholds in static noise. In: *CGIV 2004 - Second European Conference on*  
559 *Color in Graphics, Imaging, and Vision and Sixth International Symposium on*  
560 *Multispectral Color Science*, 2004.  
561
- 562 [51] H. Liu, M. Huang, G. Cui, M.R. Luo, M. Melgosa, Color-difference evaluation for  
563 digital images using a categorical judgment method, *J Opt Soc Am A Opt Image Sci*  
564 *Vis* 30(4) (2013) 616-626.  
565
- 566 [52] B. Prieto, B. Silva, N. Aira, L. Laiz, Induction of biofilms on quartz surfaces as a  
567 means of reducing the visual impact of quartz quarries, *Biofouling* 21 (2005) 237–246.  
568
- 569 [53] E. Valencia Díaz, *Procesado de imagen digital en color: Adquisición, Análisis*  
570 *Colorimétrico y Realce* (In Spanish). PhD Thesis, *Universitat Politècnica de Catalunya*,  
571 *Spain*, 2007.  
572

573 [54] J. Schanda, Colorimetry: Understanding the CIE system. John Wiley & Sons: New  
574 York, 2007.

575

576 [55] P. Sanmartín, Evaluación de dos tratamientos consolidantes aplicados a granitos y  
577 calcarenitas (In Spanish). Supervised research project, Universidade de Santiago de  
578 Compostela, Spain, 2007.

579

580 [56] B. Prieto, B. Silva, Estimation of the potential bioreceptivity of granitic rocks from  
581 their intrinsic properties, Int Biodeter Biodegr 56 (2005) 206–215.

582

583

584

585 **Capture figures:**

586

587 **Figure 1.** Image acquisition system and PL-A782 CMOS digital camera.

588 **Figure 2.** Camera settings.

589 **Figure 3.** Control for lighting or illuminance level (in lx).

590 **Figure 4.** Total color difference ( $\Delta E^*_{ab}$ ) for the six commercial varieties of granite,  
591 obtained with both devices: spectrophotometer and camera.

Figure 1

PL-A782  
MV Camera



Figure 2

Video Capture	Descriptors	External Control	Callbacks	Extended Shutter
Basic Controls	LUT and FFC	Region of Interest	Image Capture	
Camera Select PixelINK Camera s/n : 782000508		Video Preview Play Pause Stop		
Exposure Time (ms) 0.063 99.537 Auto 2000		Gain (dB) 0 0 Auto 22.1		
Saturation (%) 0 100 Auto 250		Brightness (%) 0 0 Auto 100		
Gamma <input type="checkbox"/> [On] 0.1 2.2 Auto 4		Frame Rate (fps) <input type="checkbox"/> [On] 2 20.8905 Auto 20.9035		
White Balance Red 1.09766 Green 1 Blue 1.41016 0 Auto 4		Color Temp. (K) <input type="checkbox"/> [On] 3200 5000 6500		
		Size 888 x 1608 ...		
Image Capture File Name: C:\Documents and Settings\Edafologia\Escritorio\prueba.tif Browse				
File Format: Tiff No. of Frames: 1 Capture				
<input checked="" type="checkbox"/> Capture Full Frame <input type="checkbox"/> Increment File Name After Capture				
<input checked="" type="checkbox"/> Capture Full Resolution <input checked="" type="checkbox"/> Preview Image After Capture				

Figure 3

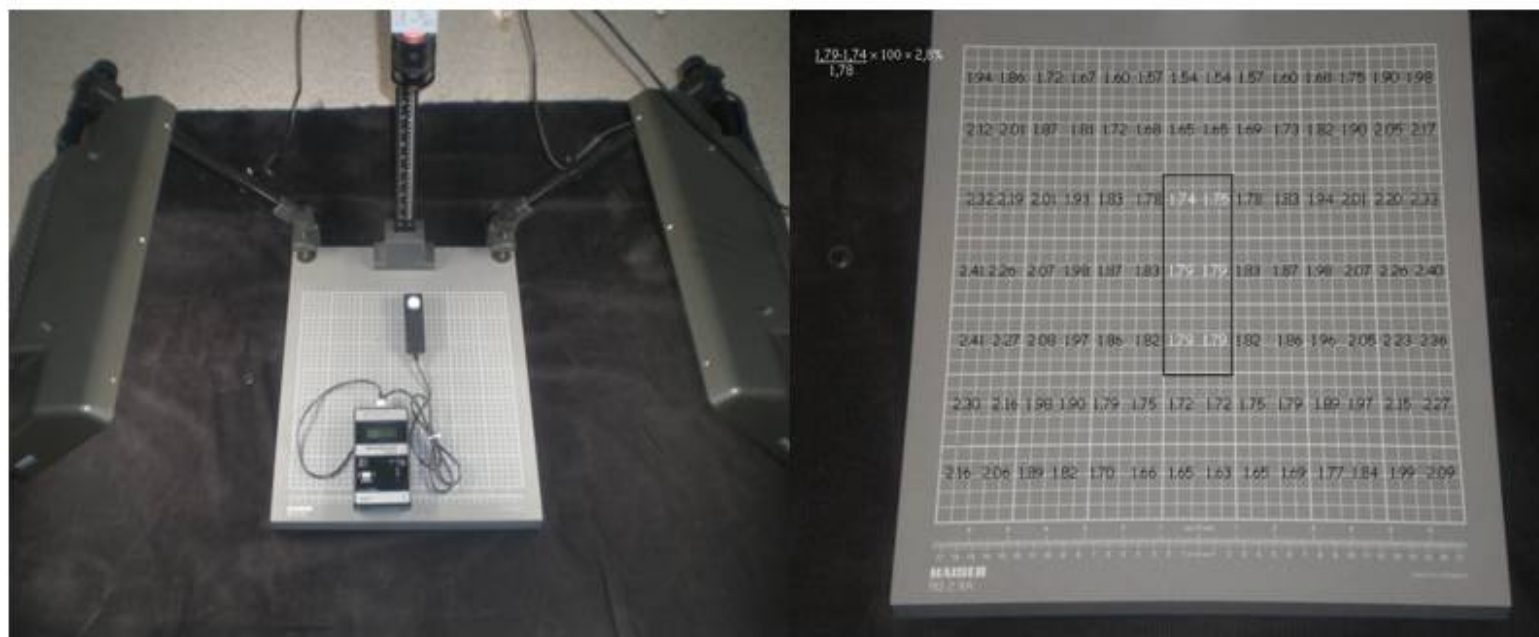
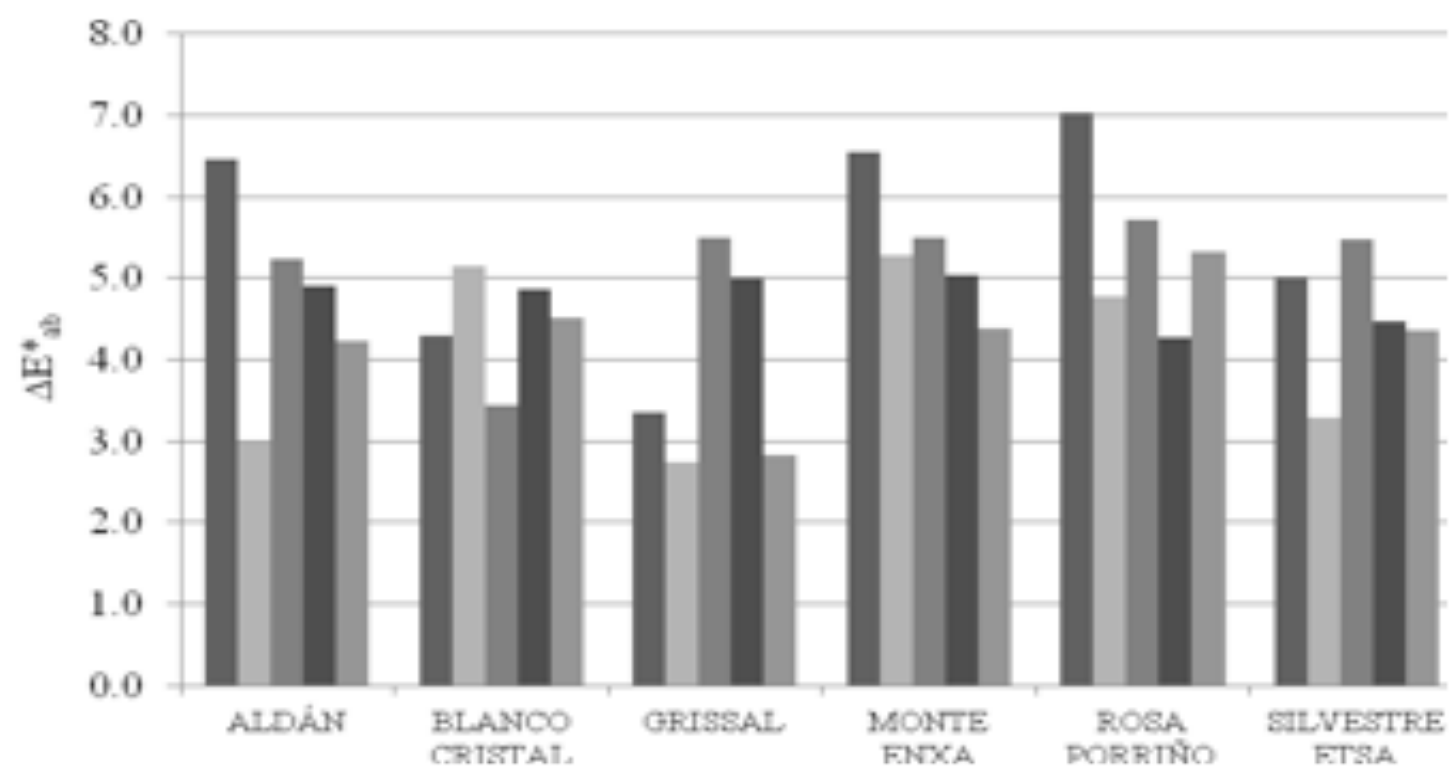


Figure 4



1 **Table 1.** Mineralogical and petrographic features of the types of granite under study.

2

3

Granite name	Location of Quarry	Macroscopic Aspect / Classification and Geochemistry	Textural Characteristics	Mineral Composition
<i>Aldán</i>	Area of Morrazo (Pontevedra, Spain)	Yellow-white, medium-, coarse-grained / Micaceous calcalkaline granite	Granoblastic heterogranular of coarse grain	Quartz (35%), Feldspar-K (21%), Plagioclases (23%), Biotite (10%), Moscovite (10%)
<i>Blanco Cristal</i>	Cadalso de los Vidrios pluton (Madrid, Spain)	White, medium-grained / Biotite adamellitic granite	Heterogranular-panallatrimorphic of medium grain	Quartz (26%), Feldspar-K (29%), Plagioclases (27.5%), Biotite (9%), Moscovite (2%), Clorite (4.5%)
<i>Grissal</i>	Rivadavia pluton (Ourense, Spain)	Grey coarse-grained / Alkaline granite	Porphyritic-panallatrimorphic of coarse grain	Quartz (30.5%), Feldspar-K (34.5%), Plagioclases (17.5%), Biotite (0.6%), Moscovite (0.5%), Clorite (3.5%)
<i>Monte Enxa</i>	Area of Barbanza (A Coruña, Spain)	White, medium-, coarse-grained / Two mica granite	Heterogranular-allatrimorphic of medium-, coarse-grain	Quartz (45%), Feldspar-K (18%), Plagioclases (12%), Biotite (7%), Moscovite (17%)
<i>Rosa Porriño</i>	Porriño pluton (Pontevedra, Spain)	Pinkish, coarse-grained granite / Biotite adamellitic	Porphyritic-panallatrimorphic of coarse grain	Quartz (30%), Feldspar-K (33%),

		granite		Plagioclases (21%), Biotite (9%), Clorite (3.5%)
<i>Silvestre</i>	Area of Vigo (Pontevedra, Spain)	White medium-grained with some ochre spots due to biotite weathering / Two mica adamellitic granite	Equigranular-panallatrimorphic of medium grain	Quartz (29%), Feldespar-K (26%), Plagioclases (24%), Biotite (8%), Moscovite (8%), Clorite (3.5%)

4 Petrographic characteristics and mineral composition described in [31, 55, 56].

5

6

7 **Table 2.** Average, maximum and minimum total color differences between the  
8 measured and the estimated CIELAB color stimuli, of the 212 color patches from the  
9 glossy and matte Munsell collection. For each color difference equation, the  
10 combination of conditions yielding the best result is indicated in bold.  
11  
12

		SCI		SCE	
		8-bits	10-bits	8-bits	10-bits
$\Delta E^*_{ab}$	Average	2.0	<b>1.9</b>	1.5	1.7
	Maximum	8.7	<b>6.9</b>	9.9	10.5
	Minimum	0.1	<b>0.2</b>	0.2	0.1
$\Delta E_{94} (2:1:1)$	Average	1.2	<b>1.2</b>	1.1	1.2
	Maximum	4.4	<b>3.9</b>	5.0	5.4
	Minimum	0.1	<b>0.1</b>	0.2	0.1
$\Delta E_{94} (1:1:1)$	Average	1.8	<b>1.8</b>	1.4	1.5
	Maximum	8.7	<b>6.9</b>	9.9	10.5
	Minimum	0.1	<b>0.2</b>	0.2	0.1
$\Delta E_{00} (2:1:1)$	Average	<b>1.7</b>	1.7	1.4	1.5
	Maximum	<b>3.8</b>	4.1	4.5	4.6
	Minimum	<b>0.1</b>	0.1	0.1	0.1
$\Delta E_{00} (1:1:1)$	Average	1.7	<b>1.7</b>	1.4	1.5
	Maximum	6.5	<b>5.8</b>	6.3	6.7
	Minimum	0.1	<b>0.2</b>	0.2	0.1
<b>CMC (2:1)</b>	Average	1.1	<b>1.1</b>	1.1	1.3
	Maximum	3.9	<b>3.7</b>	8.0	8.4
	Minimum	0.1	<b>0.1</b>	0.1	0.1
<b>CMC (1:1)</b>	Average	1.5	<b>1.5</b>	1.4	1.5
	Maximum	7.8	<b>6.3</b>	15.8	16.4
	Minimum	0.1	<b>0.2</b>	0.2	0.1

14 **Table 3.** Absolute and relative discrepancies between the spectrophotometer and the  
15 digital camera in the measurement of  $\Delta E^*_{ab}$  total color difference.

16  
17

	Absolute Discrepancy $D_i$	Relative Discrepancy $D_i^r$
Average $\pm$ SD	1.32 $\pm$ 1.06	0.06 $\pm$ 0.08
Maximum	6.41	0.84
Minimum	0.00	0.00

18

19 **Table 4.** Summary table of precision and tolerance (in CIELAB units) of the  
20 instrumental devices used.

21

22

	$n\Delta E^*_{ab}$ (Precision)	Instrumental tolerance
Spectrophotometer	0.01	0.1
Digital camera	0.24	2.4

23